Complex nonlocal optical potential for neutron scattering from ^{208}Pb

Amos Lev* and William P. Beres*
Wayne State University, Detroit, Michigan 48202

and

M. Divadeenam†
Duke University and Triangle Universities Nuclear Laboratory, Durham, North Carolina 27706
(Received 11 February 1974)

A nonlocal energy-dependent imaginary optical potential is calculated for neutron scattering from ^{208}Pb in the intermediate structure model with weak particle-vibration coupling. The energy range studied is 0–12 MeV and the partial waves considered are $l=0$–4. The corresponding contribution to the real potential has also been obtained and is relatively small; this potential is presented for s waves. The imaginary potential is used to calculate the absorption cross section in this energy range for each partial wave. Both compound-nucleus and inelastic contributions to the potential and the absorption cross section are included. Below 5 MeV compound-nucleus contributions are dominant. Above this energy inelastic excitations based on single-particle resonances and compound-nucleus states based on giant resonances contribute, with the former being more significant. A comparison of the calculated absorption to experiment for s, p, d, and f waves is made below the inelastic threshold of 2.6 MeV. The agreement, except for p waves, is quite good in terms of the number of resonances and other significant details of the cross section. The calculated absorption cross sections up to 12 MeV are compared to the results from a phenomenological local surface-peaked imaginary potential. The nonlocal potential is also surface peaked and the details of its radial behavior for an arbitrary energy are given in a contour plot.

[NUCLEAR REACTIONS ^{208}Pb(n,n), $E=0$–12 MeV; calculated nonlocal imaginary optical potential and absorption. Comparison with experiment and with a local imaginary potential. Particle-vibration doorways.]

I. INTRODUCTION

The optical model reduces the nuclear many-body scattering problem to the simpler one of single-particle scattering in a complex well. It is an attempt to explain the existence of observed broad resonances in nucleon-nucleus scattering. These resonances are in addition to those of the sharp narrow compound-nuclear type. In recent years the optical model has become an important tool for both theoretical and experimental nuclear physicists. However, despite its fundamental importance, the major efforts (with a few exceptions) have been toward a phenomenological fitting of the scattering data, e.g., Refs. 1–5.

It is clear that a generally applicable and acceptable theoretical formulation of the optical model is necessary in order to answer many of the interesting physical questions which research suggests. In this paper we obtain a significant portion of the neutron optical potential—primarily the imaginary part, which is quite interesting because it involves the dynamics of the system.

Our work is based on a detailed analysis of the nucleon-nucleus system. In particular, we explicitly take into account specific modes of nuclear excitation during the scattering process. These modes are usually considered in detail only in describing the resonant part of the cross section, but we show that their description is very important in determining the so-called average potential available to the incident nucleon. We generate a nonlocal energy-dependent potential using the intermediate structure (or doorway) model with particle-vibration coupling. The use of vibrational modes is consistent with the assumption that at low energies the imaginary part of the optical potential is peaked near the nuclear surface.

Other nuclear structure calculations of the imaginary optical potential have been done by Slanina,[6] Bruneau and Vinh-Mau,[7] Payne,[8] Cugnon,[9] O'Dwyer, Kawai, and Brown,[10] Rao, Reeves, and Satchler,[11] Satchler,[12] and Azziz and Méndez-Plácido.[13] References 6 and 7 use the G-matrix approach, Ref. 8 employs the Brueckner K-matrix technique, and Refs. 6–8 use particle-hole excitations. Ref. 9 employs the shell model theory of nuclear reactions.[14] Our work is closest in spirit to that of

Refs. 10–13. The present calculation differs from these papers in that we include both bound and continuum particles in constructing our intermediate states, and obtain neutron cross sections which are compared to experiment over an energy range. We also study the radial dependence of the potential. In a preliminary paper[15] we treated only s-wave neutron scattering. We now consider that problem in much more detail and extend our calculations to higher partial waves. Since the particle-vibration model has enjoyed much success in the Pb region and because of the simple shell features of ^{208}Pb, the case of elastic neutron scattering from ^{208}Pb is taken as an example.

The theory is described in Sec. II; Sec. III gives the results, and Sec. IV provides a discussion and conclusions.

II. THEORY

The radial part of the Schrödinger equation for a particle in a state of angular momentum lj and energy E may be written as

$$E\psi_{ljE}(r) = \int_0^\infty h(r, r')\psi_{ljE}(r')r'^2 dr', \tag{1}$$

where $h(r, r')$ is a nonlocal Hamiltonian. This Hamiltonian could also be energy- and angular-momentum-dependent. In Feshbach reaction theory[16] the Hamiltonian for the elastic scattering of a nucleon is

$$h_{ljE}(r, r') = \langle r, lj | \{H_{PP} + H_{PQ}(E^+ - H_{QQ})^{-1}H_{QP}\} | r', lj\rangle, \tag{2}$$

where P and Q are the usual continuum-space and compound-space projection operators, respectively, H is the many-body Hamiltonian for the $A+1$ particle system, and $H_{PP} = PHP$, etc. The channel vector $|r', lj\rangle$ is written in the notation of Auerbach *et al.*[17] and describes the scattering state of a particle in the continuum with angular momentum lj and energy E at the radial coordinate r'. *The radial wave function is not included in* $|r', lj\rangle$. The state $\langle r, lj|$ is defined similarly. The Hamiltonian $h_{ljE}(r, r')$ in Eq. (2) is useful for fine structure studies in that it contains many resonances due to the influence of the Q space modes. To obtain the Hamiltonian $h^{\rm opt}_{ljE}(r, r')$ appropriate for intermediate structure we replace E by $E + \frac{1}{2}iI$, where I is an energy-averaging interval. If we assume that H_{QQ} is diagonal in the compound nucleus states $|q\rangle$, Eq. (2) becomes

$$\begin{aligned} h^{\rm opt}_{ljE}(r, r') &= \langle r, lj | H_{PP} | r', lj\rangle \\ &\quad + \sum_q \frac{\langle r, lj | H_{PQ} | q\rangle\langle q | H_{QP} | r', lj\rangle}{E - E_q + \frac{1}{2}iI} \\ &\equiv \mathcal{K}_0(r, r') + \Delta V(r, r'), \end{aligned} \tag{3}$$

where $H_{QQ}|q\rangle = E_q|q\rangle$. In defining $\mathcal{K}_0$ and ΔV the labels ljE have been temporarily suppressed. The first term $\mathcal{K}_0$ is that part of the optical Hamiltonian that represents the scattering of the nucleon by the average field of the target in its ground state and is assumed to be real. This part may vary slowly with energy and its calculation involves the details of Brueckner-Hartree-Fock theory. We do not attempt such a calculation here. The second term ΔV has a more dramatic energy dependence, involves excitations of the $A+1$ compound-nucleus system, and is complex. A phenomenological local potential of the Woods-Saxon-type $V_{\rm WS}$ is usually taken to represent the nonlocal real potential and we assume that

$$V_{\rm WS} \simeq (\mathcal{K}_0 - T) + {\rm Re}(\Delta V), \tag{4}$$

where T is the kinetic energy of the scattered particle. We associate the imaginary part of ΔV with the phenomenological imaginary potential employed in the literature.[1–5] However, while most such potentials have a smooth energy dependence, Eq. (3) clearly indicates that that should not be the case. In this paper we calculate both the real and imaginary parts of ΔV.

We now assume the weak-coupling particle-vibration model of Mottelson[18] so that

$$H_{PQ} = H^\dagger_{QP} = -K(r)\sum_{\lambda\mu}\left(\frac{\hbar\omega_\lambda}{2C_\lambda}\right)^{1/2}(b_{\lambda,\mu} + (-1)^\mu b^\dagger_{\lambda,-\mu})Y_{\lambda\mu} \tag{5}$$

where $K(r)$ is a form factor, λ and μ are quantum numbers which represent, respectively, the angular momentum and its z projection for a phonon; b and $b^\dagger$ are one-phonon annihilation and creation operators, respectively, $Y_{\lambda\mu}$ is a spherical harmonic, and $(\hbar\omega_\lambda/2C_\lambda)^{1/2}$ is a phonon vibration amplitude in the target nucleus that may be obtained from the experimental literature. The quantity $K(r)$ is given by

$$K(r) = -r\frac{dV(r)}{dr}, \tag{6}$$

where $V(r)$ is the real central potential. In this paper we take $V(r) = V_{\rm WS}$. The interaction Eq. (5) limits the sum over q in ΔV [Eq. (3)] to doorway states, i.e., states one step more complicated than single particle; specifically these are particle-vibration levels.

The matrix elements which appear in ΔV involve only integration over angle in that, as mentioned earlier, the channel vectors $\langle r, lj|$ do not include the radial wave function of the scattered nucleon.

Specifically, for an even-even 0^+ target

$$\langle r, lj|H_{PQ}|q\rangle \equiv \langle r, lj|H_{PQ}|[\lambda(\alpha l'j')]j\rangle$$
$$= (2j+1)^{-1/2}\left(\frac{\hbar\omega_\lambda}{2C_\lambda}\right)^{1/2}$$
$$\times \langle lj\| Y_\lambda \| l'j'\rangle \phi_{\alpha l'j'}(r)K(r), \quad (7)$$

where $\phi_{\alpha l'j'}(r)$ is the radial wave function of the coupled single particle with quantum numbers $\alpha l'j'$. This particle may be bound ($\alpha = n$ = principal quantum number) or unbound ($\alpha = E'$ = particle energy). These two types of particles, when coupled to vibrations, represent two distinct classes of doorways. The sum in ΔV splits into a finite sum over doorways containing a coupled bound particle and into an integral over doorways containing a coupled continuum particle. Inserting the matrix element, Eq. (7), into ΔV, Eq. (3), the result is

$$\Delta V_{ljE}(r,r') = (2j+1)^{-1}K(r)K(r')\sum_\lambda \frac{\hbar\omega_\lambda}{2C_\lambda}\sum_{l'j'}|\langle lj\| Y_\lambda \| l'j'\rangle|^2$$
$$\times\left\{\sum_n \frac{\phi_{nl'j'}(r)\phi_{nl'j'}(r')}{E-E_\lambda-E_{nl'j'}+\frac{1}{2}iI} + \int_0^\infty \frac{\phi^*_{E'l'j'}(r)\phi_{E'l'j'}(r')\rho(E')}{E-E_\lambda-E'+\frac{1}{2}iI}dE'\right\}, \quad (8)$$

where E_q becomes $E_\lambda + E_{nl'j'}$ for the finite sum and $E_\lambda + E'$ for the integral. The symbols E_λ and $E_{nl'j'}$ represent respectively the vibration energy and the energy of the coupled bound single particle. The density of continuum states is given by $\rho(E')$. The energy E_λ is relative to the target ground state while all other energies are relative to threshold (i.e. target in ground state and odd nucleon at infinity). The energy $E_{nl'j'}$ is therefore always negative while all other energies are positive. The continuum wave function behaves asymptotically as

$$\phi_{E'l'j'}(r) \xrightarrow[r\to\infty]{} e^{i\delta_{l'j'}}(k'r)^{-1}\sin(k'r - \tfrac{1}{2}\pi l' + \delta_{l'j'}), \quad (9)$$

where $k' = (2mE')^{1/2}/\hbar$ is the wave number and $\delta_{l'j'}$ is the phase shift. Equation (8) illustrates that the energy behavior of both the sum and integral depends on whether E is less than or greater than a given E_λ. If $E < E_\lambda$, then the finite sum has resonances whenever $E - E_\lambda = E_{nl'j'}$. The integral in this case is expected to be small since $E - E_\lambda - E'$ never vanishes. If $E \geq E_\lambda$, then the quantity $E - E_\lambda - E_{nl'j'}$ is always positive and the finite sum is therefore expected to be small. However, the quantity $E - E_\lambda - E'$ could vanish in this case so that the integral may give a large contribution.

We now consider the evaluation of the integral in Eq. (8). It is expected to be a smooth function of energy even before averaging, unless the coupled single-particle continuum wave function $\phi_{E'l'j'}$ has a resonance. It is possible to treat such a single-particle resonance term as a bound state by using a harmonic-oscillator wave function. The appropriate term could then be extracted from the integral and placed in the finite sum of Eq. (8). In the absence of such single-particle resonances the size of I in the integral is not important. Therefore I may be treated as a vanishingly small quantity and the principal value theorem can be employed to evaluate the integral.[19] It is convenient to define

$$\mathcal{E}_\lambda = E - E_\lambda. \quad (10)$$

The integral then becomes

$$\text{Int} = \mathcal{P}\int_0^\infty \frac{\phi^*_{E'l'j'}(r)\phi_{E'l'j'}(r')\rho(E')}{\mathcal{E}_\lambda - E'}dE'$$
$$- i\pi\phi^*_{\mathcal{E}_\lambda l'j'}(r)\phi_{\mathcal{E}_\lambda l'j'}(r')\rho(\mathcal{E}_\lambda)\Theta(\mathcal{E}_\lambda), \quad (11)$$

where $\mathcal{P}$ represents the principal value of the integral and $\Theta(\mathcal{E}_\lambda)$ is a unit step function defined by

$$\Theta(\mathcal{E}_\lambda) = \begin{cases} 0, & \mathcal{E}_\lambda \leq 0, \\ 1, & \mathcal{E}_\lambda > 0. \end{cases} \quad (12)$$

If one uses a real potential, e.g., V_{WS}, to generate the continuum wave functions of the coupled nucleon, then $\phi^*_{\mathcal{E}_\lambda l'j'}(r)\phi_{\mathcal{E}_\lambda l'j'}(r')$ is real, and the real and imaginary parts of ΔV [Eq. (8)] become

$$\text{Re}[\Delta V_{ljE}(r,r')] = (2j+1)^{-1}K(r)K(r')\sum_\lambda \frac{\hbar\omega_\lambda}{2C_\lambda}\sum_{l'j'}|\langle lj\| Y_\lambda \| l'j'\rangle|^2$$
$$\times\left[\sum_n \frac{(\mathcal{E}_\lambda - E_{nl'j'})\phi_{nl'j'}(r)\phi_{nl'j'}(r')}{(\mathcal{E}_\lambda - E_{nl'j'})^2 + \frac{1}{4}I^2} + \mathcal{P}\int_0^\infty \frac{\phi^*_{E'l'j'}(r)\phi_{E'l'j'}(r')\rho(E')}{\mathcal{E}_\lambda - E'}dE'\right] \quad (13a)$$

and

$$W_{ljE}(r,r') \equiv \mathrm{Im}[\Delta V_{ljE}(r,r')]$$

$$= -(2j+1)^{-1}K(r)K(r') \sum_{\lambda} \frac{\hbar\omega_\lambda}{2C_\lambda} \sum_{l'j'} |\langle lj \| Y_\lambda \| l'j' \rangle|^2$$

$$\times \left\{ \tfrac{1}{2} \sum_n \frac{I \phi_{nl'j'}(r)\phi_{nl'j'}(r')}{(\mathcal{E}_\lambda - E_{nl'j'})^2 + \frac{1}{4}I^2} + \pi \phi^*_{\mathcal{E}_\lambda l'j'}(r)\phi_{\mathcal{E}_\lambda l'j'}(r')\rho(\mathcal{E}_\lambda)\Theta(\mathcal{E}_\lambda) \right\}. \tag{13b}$$

In Eqs. (13) the E dependence of W is implicit in the dependence on $\mathcal{E}_\lambda$ as defined in Eq. (10). We interpret the finite sum in Eqs. (13) as the contribution from *compound-nucleus formation*, whereas the second terms relate to *inelastic target excitations*. These interpretations are appropriate in that while the target is excited in both cases, the odd nucleon is bound in the former case and unbound in the latter. The finite sum in Re (ΔV), Eq. (13a), is expected to be small because of possible fluctuations in sign of the numerator. In addition, each term in this sum is identically zero at those energies that produce a resonance in the imaginary potential. We will consider Re (ΔV) later in the paper, and will now concentrate on the imaginary potential W. It is clear from Eq. (13b) that the finite-sum part of W vanishes if I becomes zero. This indicates that the compound-nucleus contribution to W is merely the result of the averaging procedure, whereas the inelastic contributions are independent of I. Clearly the potentials in Eqs. (13) are complicated objects in that they are not only nonlocal but also depend on energy and angular momentum. In addition to the explicit dependence on lj, these quantum numbers also determine the allowed doorways via angular-momentum and parity selection rules. Since the form factor $K(r)$, Eq. (6), is quite sharply peaked at roughly the nuclear surface R, we expect $K(r)$ rather than the single-particle wave functions to determine the dominant shape characteristics of the radial dependence of ΔV. Therefore, $\Delta V(r,r')$ should be peaked in the region where $r \approx r' \approx R$.

We will use the imaginary potential $W(r,r')$ to calculate the absorption (compound elastic) cross section. For a local potential $W(r)$ the quantity $-2W(r)/\hbar$ gives the absorption rate at position r. The absorption cross section in this case satisfies

$$\sigma_{\mathrm{abs}} \propto \int \Psi^*(\vec{r})W(r)\Psi(\vec{r})d\vec{r}, \tag{14}$$

where $\Psi(\vec{r})$ is the wave function of the nucleon. By analogy the absorption cross section of a particle with quantum numbers ljE in the nonlocal imaginary potential $W_{ljE}(r,r')$ is

$$\sigma_{\mathrm{abs}}^{ljE} = \frac{-2}{\hbar v} \int\int \chi^*_{ljE}(r)W_{ljE}(r,r')\chi_{ljE}(r')r^2 r'^2\, dr\, dr', \tag{15}$$

where χ_{ljE} is the radial wave function of the scattered nucleon and v is its velocity. The integral over angles is not done here because it was already performed in constructing $W_{ljE}(r,r')$, Eq. (13b). This is most clear from the discussion of the channel vector $\langle r, lj|$ which precedes Eq. (3). In fact, it is just the wave function $\chi_{ljE}(r)$ which is absent from $\langle r, lj|$. The asymptotic behavior of χ_{ljE} is similar to that of $\phi_{E'l'j'}(r)$, Eq. (9). The dependence on the wave number $k = (2mE)^{1/2}/\hbar$ is thus included in the wave functions of Eq. (15).

In principle the wave functions χ in Eq. (15) should be the solutions of the Schrödinger equation for the total optical Hamiltonian, Eq. (3). However, since ΔV is expected to be much smaller than $\mathcal{H}_0$ we make a Born approximation and obtain the scattering wave functions from a Woods-Saxon potential.

In general the scattered nucleon wave function consists of many partial waves rather than just one lj as in Eq. (15). The partial wave expansion of the scattering wave function enables one to write the absorption cross section as

$$\sigma_{\mathrm{abs}}^{E} = 4\pi \sum_{lj} (j+\tfrac{1}{2})\sigma_{\mathrm{abs}}^{ljE}, \tag{16}$$

where $\sigma_{\mathrm{abs}}^{ljE}$ is defined in Eq. (15).

III. RESULTS

We now specialize to the case of elastic neutron scattering from ^{208}Pb in the energy range 0 to 12 MeV. (At higher energies reactions other than compound elastic scattering may become important). We consider only the partial waves $s_{1/2}$, $p_{1/2}$, $p_{3/2}$, $d_{3/2}$, $d_{5/2}$, $f_{5/2}$, $f_{7/2}$, $g_{7/2}$, and $g_{9/2}$, since higher partial waves are expected to contribute insignificantly in this energy range. Specifically,

we calculate the imaginary potential W_{ljE}, Eq. (13b), the cross section σ_{abs}^{ljE}, Eq. (15), for every partial wave, and the cross section σ_{abs}^{E} [Eq. (16)]. These cross sections are compared to known experimental results in the energy range of about 0–2.6 MeV. The potential Re(ΔV) has also been calculated and the results are given for $s_{1/2}$ scattering.

The available bound coupled single neutrons are $2g_{9/2}, \ldots, 3d_{3/2}$. In addition, all allowed states are considered for the continuum coupled single particle. Table I lists the energies $E_{nl'j'}$ of the bound states as obtained from Blomqvist and Wahlborn.[20] In addition, three single-particle resonances (SPR) are found for the coupled neutron, viz., $h_{11/2}$, $k_{17/2}$, and $j_{13/2}$, and their energies are also listed. When treated as bound states (for example in our case by using harmonic-oscillator wave functions) these states may be associated with $2h_{11/2}$, $1k_{17/2}$, and $1j_{13/2}$. The wave functions of the bound states $2g_{9/2}, \ldots, 3d_{3/2}$ are obtained from a Woods-Saxon well with a spin-orbit term. The parameters were taken from Ref. 20 and are $V_0 = 44$ MeV, $R = 1.27A^{1/3}$ fm, $a = 0.67$ fm, and $V_{so} = 7.75$ MeV. To obtain the continuum wave functions (for both the coupled neutron and the scattered neutron) we used the same real potential well but allowed a slight energy dependence of the depth, viz., $V_0 = (44 - 0.3E)$ MeV.

We used the experimentally known vibrations in ^{208}Pb, including the giant dipole and the recently discovered giant quadrupole.[21] The vibrations are described in Table II. Column 1 gives the spin and parity of the vibration. The subscripts in this column distinguish states of the same spin and parity. Column 2 lists the energy E_λ, column 3 contains the electric transition strength G_λ in Weisskopf units (W.u.), and the last column lists the quantity $(\hbar\omega_\lambda/2C_\lambda)^{1/2}$ for each state as obtained by

$$\left(\frac{\hbar\omega_\lambda}{2C_\lambda}\right)^{1/2} = \frac{(4\pi G_\lambda)^{1/2}}{Z(\lambda+3)} . \tag{17}$$

The energies and G_λ values of the low-lying states are taken from Divadeenam and Beres[22] as obtained from experiment. The last two states in the table are the giant quadrupole and dipole resonances. The strength of the giant quadrupole state is calculated from the $T = 0$ energy-weighted sum rule,[23] and the strength of the giant dipole state is obtained from the $J = T = 1$ energy-weighted sum rule.[24]

Table III presents the possible doorway states for each partial wave lj. Listed are only those states where the coupled particle is in a bound state or is a single-particle resonance. While the other states with a continuum-coupled particle are not listed they were, however, used in the calculations. Column 1 gives a numerical reference label to each state, column 2 lists the lj of the scattering state, columns 3 and 4 give, respectively, the quantum numbers of the vibration and the coupled single particle. Column 5 lists the resultant doorway energy $E_d = E_\lambda + E_{nl'j'}$, and the last column gives 10^6 times the dimensionless quantity $S_{\lambda,l'j'}^{lj} = (2j+1)^{-1}(\hbar\omega_\lambda/2C_\lambda)|\langle lj \| Y_\lambda \| l'j' \rangle|^2$. It is clear from Eq. (8) that $S_{\lambda,l'j'}^{lj}$ is a measure of the strength of the doorway. We concentrate our attention now on the imaginary optical potential. In calculating the potential and cross section up to 12 MeV, the averaging interval I was taken as 0.75 MeV for all doorways except those based on the giant dipole and quadrupole resonances. Because the giant resonances are rather broad a larger value of $I = 2$ MeV was used. While I has no specific label

TABLE I. Single-particle constituents of the doorways. The bound-state energies are taken from Blomqvist and Wahlborn (Ref. 20). The last three states are single-particle resonances. See text for details.

$nl'j'$	$E_{nl'j'}$ (MeV)
$2g_{9/2}$	−3.683
$1i_{11/2}$	−2.955
$3d_{5/2}$	−1.820
$1j_{15/2}$	−1.722
$4s_{1/2}$	−1.224
$2g_{7/2}$	−0.669
$3d_{3/2}$	−0.604
$2h_{11/2}$ (SPR)	+3.000
$1k_{17/2}$ (SPR)	+6.499
$1j_{13/2}$ (SPR)	+6.708

TABLE II. Vibrations in ^{208}Pb. The spin and parity, energy, and strength are given in the first three columns, respectively. The numerical subscripts in column 1 distinguish between vibrations of the same spin and parity. The last column is obtained from Eq. (17). See text for details.

λ^π	E_λ (MeV)	G_λ (W.u.)	$\left(\frac{\hbar\omega_\lambda}{2C_\lambda}\right)^{1/2}$
3^-	2.614	39.5	0.045
5_1^-	3.198	14.0	0.020
5_2^-	3.709	1.85	0.007
2_1^+	4.070	8.00	0.024
4^+	4.305	15.00	0.024
6^+	4.405	5.5	0.011
8^+	4.600	4.00	0.008
2_2^+	11.5	96.0	0.085
1^-	13.5	13.7	0.040

TABLE III. The possible particle-vibration doorway states. The first column contains a numerical identification label for each doorway. The second column specifies the partial wave lj of the scattered nucleon. The vibration and particle constituent of each doorway are given, respectively, in columns 3 and 4. The numerical subscripts in column 3 distinguish between vibrations of the same spin and parity. The letters SPR in column 4 denote a single-particle resonance. The doorway energies $E_d = E_\lambda + E_{n'l'j'}$ are given in column 5. The last column gives 10^6 times the dimensionless strength $S^{lj}_{\lambda,l'j'}$. See text for details.

No.	lj	λ^π	$nl'j'$	E_d (MeV)	$10^6\times S^{lj}_{\lambda,l'j'}$	No.	lj	λ^π	$nl'j'$	E_d (MeV)	$10^6\times S^{lj}_{\lambda,l'j'}$
1	$s_{1/2}$	4^+	$2g_{9/2}$	0.622	228	36		6^+	$1j_{13/2}$ (SPR)	11.113	14
2		6^+	$1i_{11/2}$	1.450	61	37		1^-	$3d_{5/2}$	11.680	229
3		2_1^+	$3d_{5/2}$	2.250	143	38		1^-	$4s_{1/2}$	12.276	127
4		2_1^+	$3d_{3/2}$	3.446	95	39		1^-	$3d_{3/2}$	12.896	25
5		4^+	$2g_{7/2}$	3.636	182	40	$d_{3/2}$	4^+	$2g_{9/2}$	0.622	41
6		5_1^-	$2h_{11/2}$ (SPR)	6.198	195	41		6^+	$2g_{9/2}$	0.722	41
7		5_2^-	$2h_{11/2}$ (SPR)	6.709	26	42		4^+	$1i_{11/2}$	1.350	186
8		2_2^+	$3d_{5/2}$	9.680	1713	43		6^+	$1i_{11/2}$	1.450	19
9		2_2^+	$3d_{3/2}$	10.896	1142	44		2_1^+	$3d_{5/2}$	2.250	20
10		8^+	$1k_{17/2}$ (SPR)	11.100	44	45		4^+	$3d_{5/2}$	2.485	117
11	$p_{1/2}$	5_1^-	$2g_{9/2}$	−0.485	163	46		2_1^+	$4s_{1/2}$	2.846	48
12		5_2^-	$2g_{9/2}$	0.026	21	47		2_1^+	$2g_{7/2}$	3.401	122
13		5_1^-	$1i_{11/2}$	0.243	195	48		2_1^+	$3d_{3/2}$	3.466	48
14		5_2^-	$1i_{11/2}$	0.754	26	49		4^+	$2g_{7/2}$	3.636	65
15		3^-	$3d_{5/2}$	0.794	490	50		5_1^-	$2h_{11/2}$ (SPR)	6.198	38
16		3^-	$2g_{7/2}$	1.945	653	51		5_2^-	$2h_{11/2}$ (SPR)	6.709	5
17		8^+	$1j_{15/2}$	2.878	39	52		2_2^+	$3d_{5/2}$	9.680	245
18		6^+	$2h_{11/2}$ (SPR)	7.405	61	53		5_1^-	$1j_{13/2}$ (SPR)	9.906	158
19		6^+	$1j_{13/2}$ (SPR)	11.113	71	54		2_2^+	$4s_{1/2}$	10.276	571
20		1^-	$4s_{1/2}$	12.276	127	55		5_2^-	$1j_{13/2}$ (SPR)	10.417	21
21		1^-	$3d_{3/2}$	12.896	255	56		2_2^+	$2g_{7/2}$	10.831	1469
22	$p_{3/2}$	3^-	$2g_{9/2}$	−1.069	544	57		2_2^+	$3d_{3/2}$	10.896	571
23		5_1^-	$2g_{9/2}$	−0.485	54	58	$d_{5/2}$	2_1^+	$2g_{9/2}$	0.387	113
24		5_2^-	$2g_{9/2}$	0.026	7	59		4^+	$2g_{9/2}$	0.622	71
25		5_1^-	$1i_{11/2}$	0.243	38	60		6^+	$2g_{9/2}$	0.722	11
26		5_2^-	$1i_{11/2}$	0.754	5	61		4^+	$1i_{11/2}$	1.350	19
27		3^-	$3d_{5/2}$	0.794	196	62		6^+	$1i_{11/2}$	1.450	13
28		3^-	$2g_{7/2}$	1.945	109	63		5_1^-	$1j_{15/2}$	1.476	140
29		3^-	$3d_{3/2}$	2.010	294	64		8^+	$1i_{11/2}$	1.645	21
30		5_1^-	$2g_{7/2}$	2.529	108	65		5_2^-	$1j_{15/2}$	1.987	19
31		6^+	$1j_{15/2}$	2.683	57	66		2_1^+	$3d_{5/2}$	2.250	54
32		8^+	$1j_{15/2}$	2.878	12	67		4^+	$3d_{5/2}$	2.485	39
33		5_2^-	$2g_{7/2}$	3.040	14	68		2_1^+	$4s_{1/2}$	2.846	48
34		4^+	$2h_{11/2}$ (SPR)	7.305	186	69		2_1^+	$2g_{7/2}$	3.401	9
35		6^+	$2h_{11/2}$ (SPR)	7.405	19	70		2_1^+	$3d_{3/2}$	3.466	14

TABLE III *(Continued)*

No.	lj	λ^π	$nl'j'$	E_d (MeV)	$10^6 \times S^{lj}_{\lambda,l'j'}$
71	$d_{5/2}$	4^+	$2g_{7/2}$	3.636	35
72		4^+	$3d_{3/2}$	3.701	78
73		6^+	$2g_{7/2}$	3.736	31
74		3^-	$2h_{11/2}$ (SPR)	5.614	494
75		5_1^-	$2h_{11/2}$ (SPR)	6.198	58
76		5_2^-	$2h_{11/2}$ (SPR)	6.709	8
77		2_2^+	$2g_{9/2}$	7.817	1360
78		2_2^+	$3d_{5/2}$	9.680	653
79		5_1^-	$1j_{13/2}$ (SPR)	9.906	18
80		2_2^+	$4s_{1/2}$	10.276	571
81		5_2^-	$1j_{13/2}$ (SPR)	10.417	2
82		2_2^+	$2g_{7/2}$	10.831	109
83		2_2^+	$3d_{3/2}$	10.896	163
84		6^+	$1k_{17/2}$ (SPR)	10.905	50
85	$f_{5/2}$	3^-	$2g_{9/2}$	−1.069	49
86		5_1^-	$2g_{9/2}$	−0.485	33
87		3^-	$1i_{11/2}$	−0.341	494
88		5_2^-	$2g_{9/2}$	0.026	4
89		5_1^-	$1i_{11/2}$	0.243	58
90		5_2^-	$1i_{11/2}$	0.754	8
91		3^-	$3d_{5/2}$	0.794	87
92		5_1^-	$3d_{5/2}$	1.378	77
93		3^-	$4s_{1/2}$	1.390	163
94		5_2^-	$3d_{5/2}$	1.889	10
95		3^-	$2g_{7/2}$	1.945	218
96		3^-	$3d_{3/2}$	2.010	131
97		5_1^-	$2g_{7/2}$	2.529	31
98		6^+	$1j_{15/2}$	2.683	7
99		8^+	$1j_{15/2}$	2.878	9
100		5_2^-	$2g_{7/2}$	3.040	4
101		4^+	$2h_{11/2}$ (SPR)	7.305	19
102		6^+	$2h_{11/2}$ (SPR)	7.405	13
103		8^+	$2h_{11/2}$ (SPR)	7.600	21
104		4^+	$1j_{13/2}$ (SPR)	11.013	167
105		6^+	$1j_{13/2}$ (SPR)	11.113	21
106		8^+	$1j_{13/2}$ (SPR)	11.308	6
107		1^-	$3d_{5/2}$	11.680	11
108		1^-	$2g_{7/2}$	12.831	218
109		1^-	$3d_{3/2}$	12.896	153
110	$f_{7/2}$	3^-	$2g_{9/2}$	−1.069	223
111		5_1^-	$2g_{9/2}$	−0.485	38
112		3^-	$1i_{11/2}$	−0.341	29
113		5_2^-	$2g_{9/2}$	0.026	5
114		5_1^-	$1i_{11/2}$	0.243	18
115		5_2^-	$1i_{11/2}$	0.754	2
116		3^-	$3d_{5/2}$	0.794	163
117		5_1^-	$3d_{5/2}$	1.378	23
118		3^-	$4s_{1/2}$	1.390	163
119		5_2^-	$3d_{5/2}$	1.889	3
120		3^-	$2g_{7/2}$	1.945	45
121		3^-	$3d_{3/2}$	2.010	54
122		5_1^-	$2g_{7/2}$	2.529	27
123		4^+	$1j_{15/2}$	2.583	156
124		5_1^-	$3d_{3/2}$	2.594	54
125		6^+	$1j_{15/2}$	2.683	20
126		8^+	$1j_{15/2}$	2.878	8
127		5_2^-	$2g_{7/2}$	3.040	4
128		5_2^-	$3d_{3/2}$	3.105	7
129		2_1^+	$2h_{11/2}$ (SPR)	7.070	108
130		4^+	$2h_{11/2}$ (SPR)	7.305	72
131		6^+	$2h_{11/2}$ (SPR)	7.405	13
132		8^+	$2h_{11/2}$ (SPR)	7.600	4
133		5_1^-	$1k_{17/2}$ (SPR)	9.698	130
134		1^-	$2g_{9/2}$	9.817	212
135		5_2^-	$1k_{17/2}$ (SPR)	10.209	17
136		4^+	$1j_{13/2}$ (SPR)	11.013	11
137		6^+	$1j_{13/2}$ (SPR)	11.113	7
138		8^+	$1j_{13/2}$ (SPR)	11.308	8
139		1^-	$3d_{5/2}$	11.680	164
140		1^-	$2g_{7/2}$	12.831	6
141		2_2^+	$2h_{11/2}$ (SPR)	14.500	1298
142	$g_{7/2}$	2_1^+	$2g_{9/2}$	0.387	5
143		4^+	$2g_{9/2}$	0.622	18
144		6^+	$2g_{9/2}$	0.722	11
145		8^+	$2g_{9/2}$	0.917	17
146		2_1^+	$1i_{11/2}$	1.115	108
147		4^+	$1i_{11/2}$	1.350	72
148		6^+	$1i_{11/2}$	1.450	13

TABLE III *(Continued)*

No.	lj	λ^π	$nl'j'$	E_d (MeV)	$10^6\times S^{lj}_{\lambda,l'j'}$	No.	lj	λ^π	$nl'j'$	E_d (MeV)	$10^6\times S^{lj}_{\lambda,l'j'}$
149	$g_{7/2}$	5_1^-	$1j_{15/2}$	1.476	10	179		2_1^+	$1i_{11/2}$	1.115	3
150		8^+	$1i_{11/2}$	1.645	4	180		4^+	$1i_{11/2}$	1.350	11
151		5_2^-	$1j_{15/2}$	1.987	1	181		6^+	$1i_{11/2}$	1.450	6
152		2_1^+	$3d_{5/2}$	2.250	7	182		5_1^-	$1j_{15/2}$	1.476	58
153		4^+	$3d_{5/2}$	2.485	27	183		8^+	$1i_{11/2}$	1.645	6
154		6^+	$3d_{5/2}$	2.585	23	184		5_2^-	$1j_{15/2}$	1.987	8
155		4^+	$4s_{1/2}$	3.081	46	185		2_1^+	$3d_{5/2}$	2.250	68
156		2_1^+	$2g_{7/2}$	3.401	57	186		4^+	$3d_{5/2}$	2.485	43
157		2_1^+	$3d_{3/2}$	3.466	61	187		6^+	$3d_{5/2}$	2.585	6
158		4^+	$2g_{7/2}$	3.636	48	188		4^+	$4s_{1/2}$	3.081	46
159		4^+	$3d_{3/2}$	3.701	33	189		2_1^+	$2g_{7/2}$	3.401	4
160		6^+	$2g_{7/2}$	3.736	8	190		4^+	$2g_{7/2}$	3.636	15
161		3^-	$2h_{11/2}$ (SPR)	5.614	29	191		4^+	$3d_{3/2}$	3.701	17
162		5_1^-	$2h_{11/2}$ (SPR)	6.198	18	192		6^+	$2g_{7/2}$	3.736	9
163		5_2^-	$2h_{11/2}$ (SPR)	6.709	2	193		6^+	$3d_{3/2}$	3.801	17
164		2_2^+	$2g_{9/2}$	7.817	62	194		8^+	$2g_{7/2}$	3.931	13
165		2_2^+	$1i_{11/2}$	8.545	1298	195		3^-	$2h_{11/2}$ (SPR)	5.614	224
166		3^-	$1j_{13/2}$ (SPR)	9.322	466	196		5_1^-	$2h_{11/2}$ (SPR)	6.198	40
167		2_2^+	$3d_{5/2}$	9.680	82	197		5_2^-	$2h_{11/2}$ (SPR)	6.709	5
168		5_1^-	$1j_{13/2}$ (SPR)	9.906	58	198		2_2^+	$2g_{9/2}$	7.817	692
169		5_2^-	$1j_{13/2}$ (SPR)	10.417	8	199		2_2^+	$1i_{11/2}$	8.545	40
170		2_2^+	$2g_{7/2}$	10.831	680	200		3^-	$1j_{13/2}$ (SPR)	9.322	19
171		6^+	$1k_{17/2}$ (SPR)	10.905	4	201		2_2^+	$3d_{5/2}$	9.680	816
172		2_2^+	$3d_{3/2}$	10.896	734	202		5_1^-	$1j_{13/2}$ (SPR)	9.906	11
173		8^+	$1k_{17/2}$ (SPR)	11.100	5	203		5_2^-	$1j_{13/2}$ (SPR)	10.417	1
174	$g_{9/2}$	2_1^+	$2g_{9/2}$	0.387	58	204		4^+	$1k_{17/2}$ (SPR)	10.805	149
175		4^+	$2g_{9/2}$	0.622	52	205		2_2^+	$2g_{7/2}$	10.831	49
176		6^+	$2g_{9/2}$	0.722	10	206		6^+	$1k_{17/2}$ (SPR)	10.905	20
177		3^-	$1j_{15/2}$	0.892	447	207		8^+	$1k_{17/2}$ (SPR)	11.100	8
178		8^+	$2g_{9/2}$	0.917	3	208		1^-	$2h_{11/2}$ (SPR)	16.500	208

[e.g., in Eqs. (13)], we would reasonably expect it to vary depending on the doorways and energy range of interest. In considering the comparison of calculated cross sections to experiment in the range 0–2.6 MeV, smaller values of I were used to study the intermediate structure in more detail.

As mentioned in Sec. II, $\Delta V_{ljE}(r,r')$ and consequently $W_{ljE}(r,r')$ [Eq. (13b)] are peaked near $r\approx r'\approx R$, where R is the nuclear surface radius. In order to display the energy dependence in a simple way we therefore next study the energy behavior of $W_{ljE}(R,R)$. To simplify the notation and allow us to plot a positive quantity we define

$$W_0=-W_{ljE}(R,R), \tag{18}$$

where the labels ljE have been suppressed. In each subsequent plot of W_0 vs energy the appropriate lj value will be clearly specified. The results for $lj=s_{1/2}$ are given in Fig. 1(a). The solid line gives the total contribution of both the compound-nucleus formation and inelastic excitations. The dashed line represents the inelastic

contribution only. The numbers in parentheses refer to the pertinent doorway state label given in column 1 of Table III. Only the strongest contributing doorways are so denoted for each resonance. The sharp peak at 6.2 MeV, labeled (6), is due to the doorway composed of the $2h_{11/2}$ SPR and the 5_1^- vibration. The dashed-dotted line is the result of treating this SPR as a bound state, using a harmonic-oscillator wave function and $I = 0.75$ MeV.

For comparison we present the absorption vs energy in Fig. 1(b). By absorption we mean the quantity $4\pi(j+\frac{1}{2})\sigma_{\rm abs}^{ljE}$ which appears in Eq. (16).

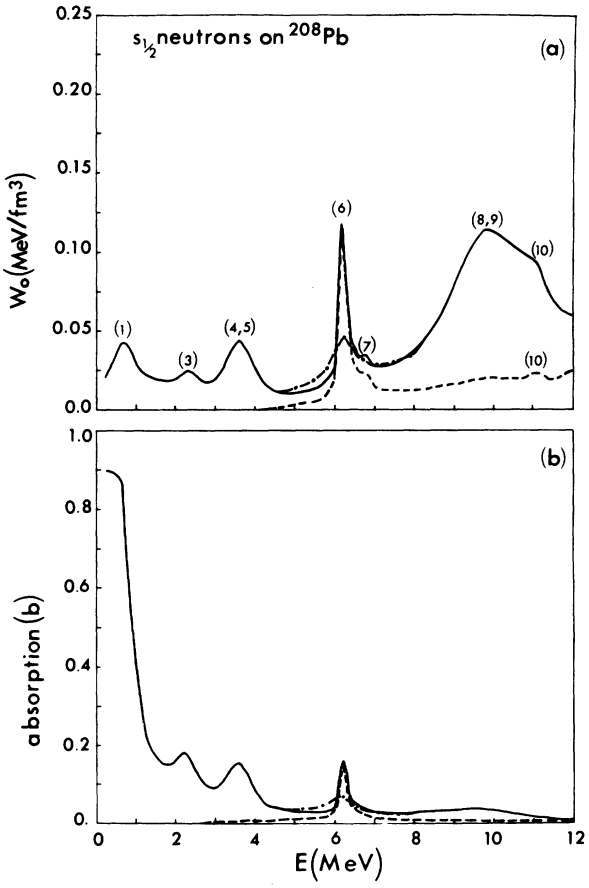

FIG. 1. Part (a) gives the imaginary potential peak W_0 [Eq. (18)] vs E for the scattering of $s_{1/2}$ neutrons. Part (b) describes the corresponding absorption $4\pi(j+\frac{1}{2})\sigma_{\rm abs}^{ljE}$ [cf. Eqs. (15) and (16)]. The value $I = 0.75$ MeV was used for all doorways except those associated with the giant resonances, where $I = 2$ MeV was used. The dashed line gives the contribution of inelastic excitations while the solid line gives the sum of inelastic excitations and compound-nucleus formation. The numbers on top of the peaks refer to the label of the pertinent doorways in Table III. The dashed-dotted line is a result of treating the $2h_{11/2}$ SPR as a bound state with $I = 0.75$ MeV.

The quantity $\sigma_{\rm abs}^{ljE}$ is defined in Eq. (15). The solid, dashed, and dashed-dotted lines are defined as in Fig. 1(a). Figures 2 through 9 give the corresponding results for the partial waves $p_{1/2}$, $p_{3/2}$, $d_{3/2}$, $d_{5/2}$, $f_{5/2}$, $f_{7/2}$, $g_{7/2}$, and $g_{9/2}$. In order to emphasize the details of the SPR's we did not treat these resonances as bound states. Therefore the dashed-dotted lines do not appear in these figures. Figure 10(a) presents simultaneously the potentials W_0 for every partial wave under consideration. Figure 10(b) gives the absorption cross section $\sigma_{\rm abs}^{E}$ [Eq. (16)] vs energy. This cross section is the sum of the absorptions for the partial waves $s_{1/2}, \ldots, g_{9/2}$. The dashed line represents the inelastic scattering only.

We now compare the calculated absorption from our nonlocal energy-dependent potential with that obtained from a phenomenological local energy-independent potential. The shape of the latter is proportional to the derivative of the previously described Woods-Saxon potential, and its strength was arbitrarily chosen as 5 MeV. Figures 11–19 give the results for the individual partial waves

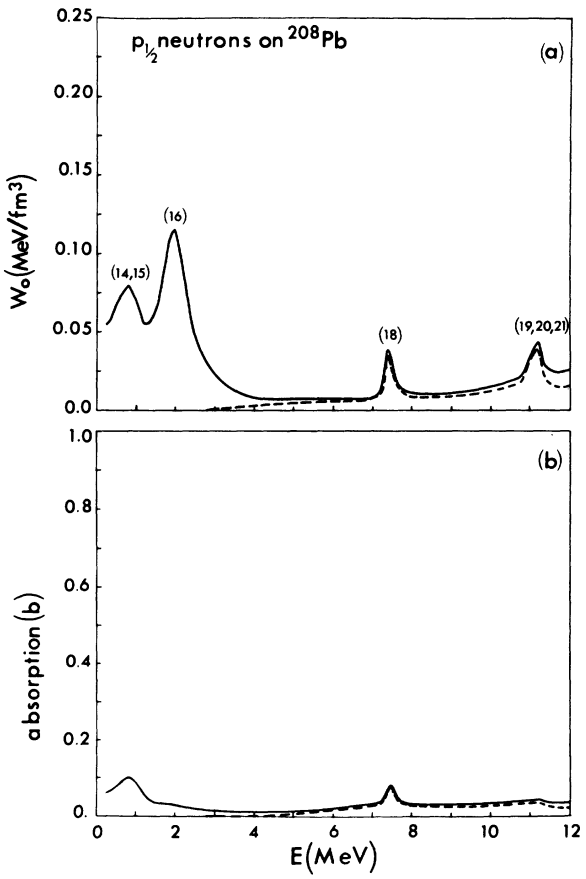

FIG. 2. Imaginary potential W_0 and absorption for $p_{1/2}$ neutrons. See Fig. 1 caption for details.

$s_{1/2}, \ldots, g_{9/2}$. The solid line in each figure is the same as in the corresponding lower portions of Figs. 1–9. The dashed curves in Figs. 11–19 represent the phenomenological absorption referred to above. Figure 20 gives the sum of the cross sections of Figs. 11–19.

We now present the results of a comparison of our calculated cross sections with experiment for energies below about 2.6 MeV, the inelastic threshold. In order to better analyze the fine structure in this small energy range we use smaller values of the averaging interval I than previously. These values are indicated in the appropriate figures. Figures 21–24 give, respectively, the comparison for s, p, d, and f partial waves. There are very little data for higher partial waves. The figures show in part (a) the quantity $\sigma_t^{(I)}$ in barns. This is the observed total cross section, i.e., it includes both potential elastic and compound (or resonance) elastic scattering, and was obtained using an R-matrix code for each partial wave with parameters determined from experiment.[25–27] In part (b) of these figures the experimental compound (resonance) elastic scattering cross section $\sigma_{\rm res}^{(I)}$ is given separately. In both these parts the word experimental is written in quotes to indicate that each partial wave cross section has been separately extracted from experiment. The calculated cross section for $lj = s_{1/2}$ is given in Fig. 21(c). In Figs. 22–24 the calculated results are presented in parts (c) and (d) for the two separate possible j values associated with each l. The numbers in parentheses above the calculated resonances refer to the pertinent doorway state label given in column 1 of Table III. Only the strongest contributing doorways are so denoted for each resonance.

In order to show a typical radial dependence of our calculated imaginary potential, we give in Fig. 25 a map of contour lines of $-W_{ljE}(r, r')$ [Eq. (13b)] for $lj = s_{1/2}$ and $E = 0.5$ MeV. The value of I is 0.75 MeV. The actual nuclear radius R is indicated in the figure as a reference point. The dashed line is a symmetry axis and the values of

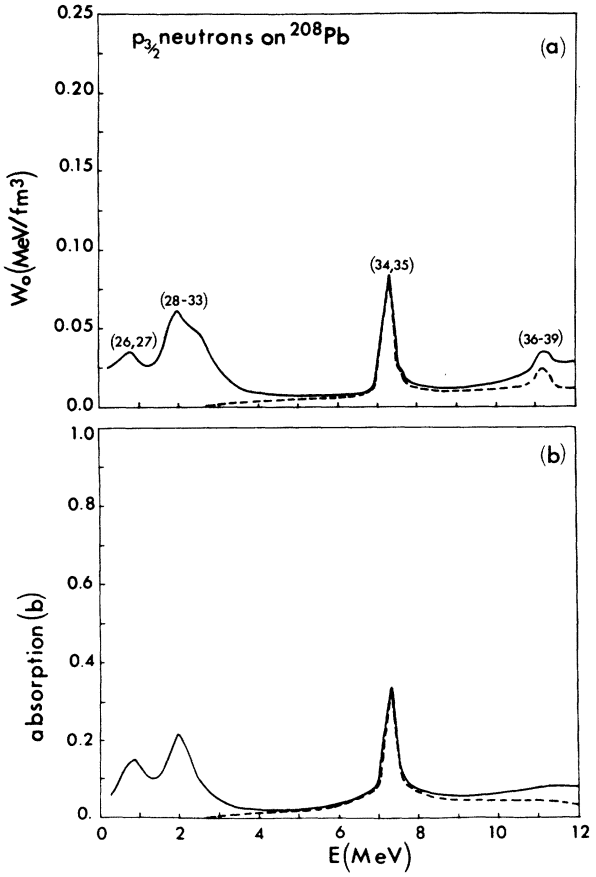

FIG. 3. Imaginary potential W_0 and absorption for $p_{3/2}$ neutrons. See Fig. 1 caption for details.

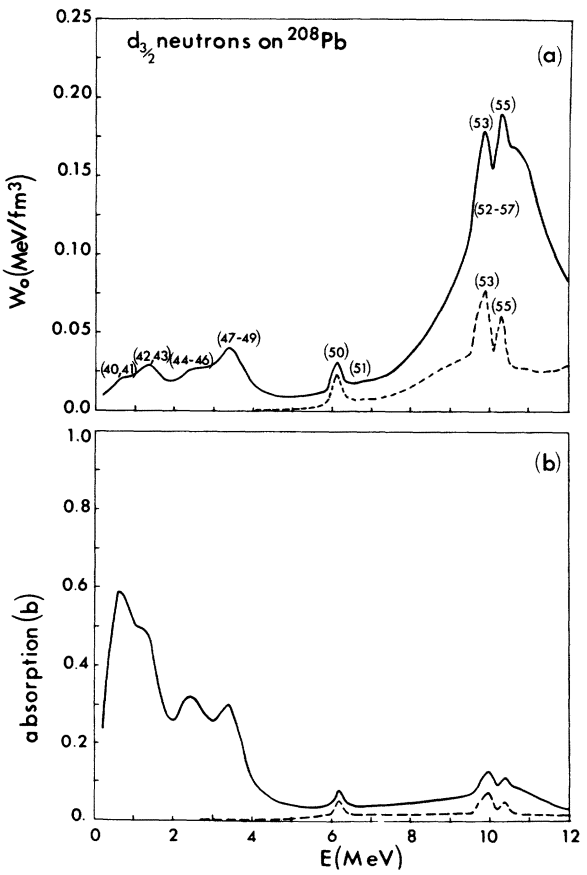

FIG. 4. Imaginary potential W_0 and absorption for $d_{3/2}$ neutrons. See Fig. 1 caption for details.

$-W$ are written near each contour.

The shape of the contour lines in Fig. 25 suggests that one may try to approximate $W_{ljE}(r,r')$ by a Gaussian peaked at the nuclear surface R and of the following form

$$W_{ljE}(r,r') = W_{ljE}(R,R) \times \exp\{-[(r-R)/\beta]^2 - [(r'-R)/\beta]^2\}, \quad (19)$$

where β is a range parameter. We found that Eq. (19) gives a good description of the potential in the range 0–12 MeV with $\beta \approx 1$ fm independent of energy. However, in our calculations we used the actual calculated potential and not Eq. (19).

Figure 26 gives a typical plot of the calculated energy dependence of the real part of the optical potential, $\mathrm{Re}[\Delta V_{ljE}(r,r')]$, Eq. (13a). As we did for the imaginary potential [see statements immediately preceding Eq. (18)] we show in this figure the quantity $\mathrm{Re}[\Delta V_{ljE}(R,R)]$ for $lj = s_{1/2}$. Only the finite sum contribution to this quantity [Eq. (13a)] has been included in the calculation. Calculations have been done for the other partial waves with similar results, but are not presented here.

IV. DISCUSSION AND CONCLUSIONS

There are several important conclusions that become apparent from the results presented in the preceding section. These are now discussed.

(1) Both the compound-nucleus formation, i.e., the finite sum in Eq. (13b) and the inelastic target excitations, the second term in Eq. (13b), contribute significantly to the imaginary potential (cf. Figs. 1–9). Below about 5 MeV the structure is due entirely to the compound-nucleus type of intermediate states. While there are many such states, especially important are those based on the 3^- vibration. The well known $4^+ \otimes 2g_{9/2}$ doorway, while not of predominant importance, is present for all even partial waves.

Above 5 MeV the major contributions to the potential come from both the inelastic excitations

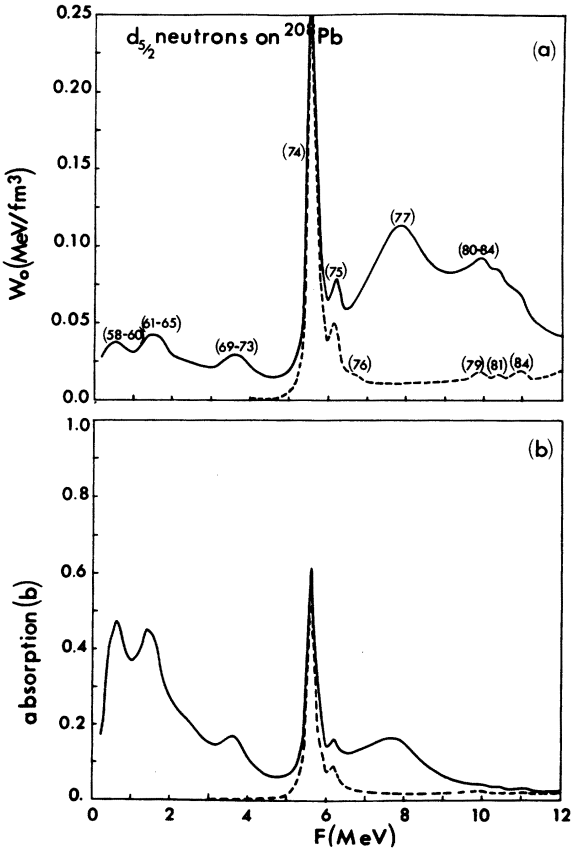

FIG. 5. Imaginary potential W_0 and absorption for $d_{5/2}$ neutrons. See Fig. 1 caption for details.

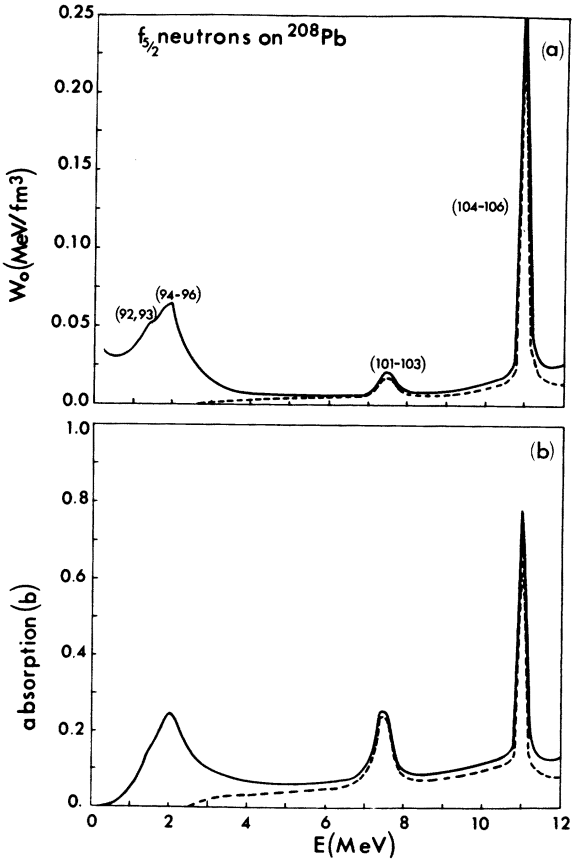

FIG. 6. Imaginary potential W_0 and absorption for $f_{5/2}$ neutrons. See Fig. 1 caption for details.

and compound-nucleus formation. The significant inelastic doorways are those containing SPR's. When the 3^- vibration can couple with an SPR it produces an especially strong inelastic contribution to the imaginary potential. In the case of compound-nucleus formation the important doorways are those based on the giant vibrations, with the giant quadrupole being much more significant than the giant dipole. States formed by a giant resonance coupled to an SPR are outside the energy range studied here.

(2) For the various partial waves studied it happens that doorways based on the $2h_{11/2}$ SPR occur at about 6–7 MeV above threshold, and those based on $1j_{13/2}$ and $1k_{17/2}$ appear about 4 MeV higher. These states are indicated by the sharp dashed peaks in Figs. 1–9. With this information it is easy to understand the general features of the potentials in Fig. 10(a). There are three fairly distinct regions. Up to about 5 MeV the potentials are due to low-lying compound-nucleus states. From about 5 to 7 MeV the structure is due to doorway states containing the $2h_{11/2}$ SPR, while at higher energies the potentials result from doorways containing either the other SPR's or giant vibrations. The same structure prevails in the total absorption cross section in Fig. 10(b). The cross sections will be discussed later in this section.

(3) The contribution of any one doorway to the potential depends on the angular momentum and parity of the partial wave of interest as well as on the properties of the doorway. An indication of these combined effects is the quantity $S^{lj}_{\lambda,l'j'}$ in Table III. In the case of SPR's the contribution to the potential can still be large even though $S^{lj}_{\lambda,l'j'}$ is small, because of the size of the intermediate single-particle radial wave function. This is true only if we do not average the SPR.

(4) Because of angular momentum selection rules the number of doorways increases with the lj value of the partial wave (cf. Table III). However, as the structure of the potential depends not only on the number of available doorways but also on their strengths, the larger number of doorways is not always reflected in the structure of the po-

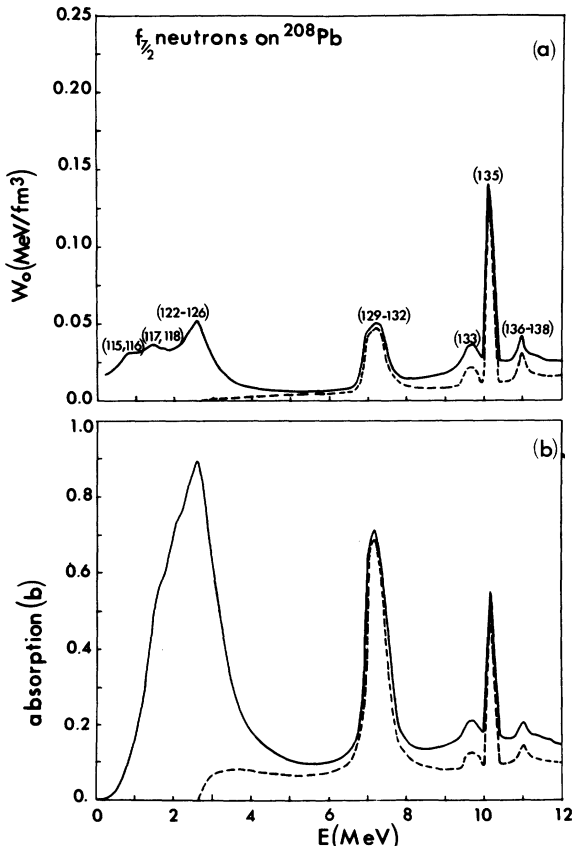

FIG. 7. Imaginary potential W_0 and absorption for $f_{7/2}$ neutrons. See Fig. 1 caption for details.

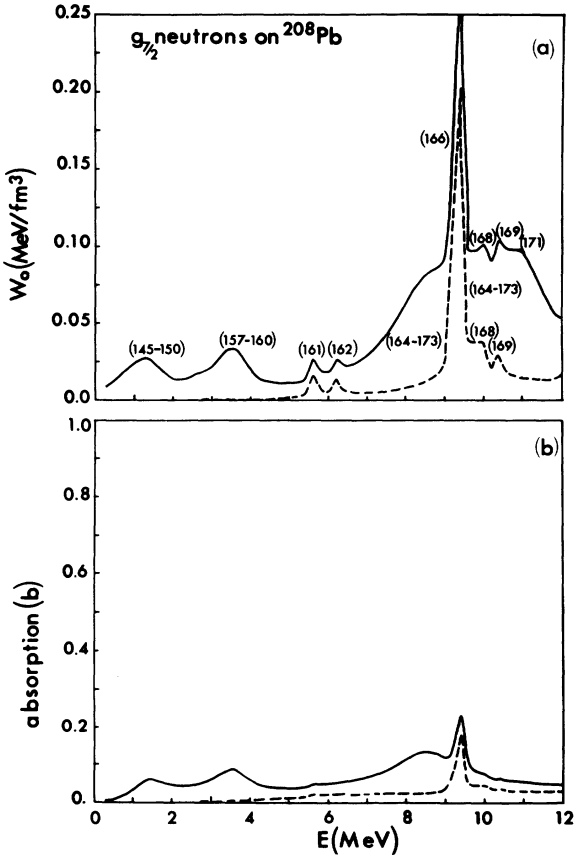

FIG. 8. Imaginary potential W_0 and absorption for $g_{7/2}$ neutrons. See Fig. 1 caption for details.

tential or the cross section.

(5) While the structure of the imaginary potential should be manifested in the absorption cross section [cf. Eq. (15)], there is no linear relationship between the two quantities. Obviously if the potential is rather large then the cross section is also expected to be large, e.g., at the energy of an SPR. However, the radial wave functions of the scattered nucleon are also quite important for the determination of the resultant cross section. Specifically, the amplitude of the wave function for a certain lj in the vicinity of the nuclear surface is energy-dependent. The closer the energy to that of a potential scattering resonance or to a bound state of the same lj, the larger the amplitude and hence the larger the absorption cross section. For example, the s-wave cross section (Fig. 1) is large at very low energies while the p-wave cross section (Figs. 2–3) is small for all energies. This is true even though the p-wave potential is larger than that for s waves at low energies. A reasonable explanation is that the $4s_{1/2}$ bound state is only 1.2 MeV below threshold while the $3p_{1/2}$ state is much more tightly bound. The absorption cross sections for d waves (Figs. 4–5) are large at low energies. This could be explained by the small binding (about 1 MeV) of the $3d_{3/2}$ and $3d_{5/2}$ wave functions.

The $2f_{5/2}$ state is bound by 8 MeV and the $3f_{5/2}$ scattering resonance is expected at about $2\hbar\omega \approx 14$ MeV above this. Thus the absorption should be large at about 6 MeV above threshold. However, the potential is quite small at this energy, thereby diminishing the cross section (Fig. 6). At somewhat higher energy the absorption does in fact show the expected behavior. The $2f_{7/2}$ state is bound by about 11 MeV so that the $f_{7/2}$ scattering wave function should be big at about 3 MeV. The absorption cross section (Fig. 7) reflects this effect. One would expect the g-wave cross sections (Figs. 8–9) to be large at low energies because the $2g_{7/2}$ and $2g_{9/2}$ states are loosely bound. How-

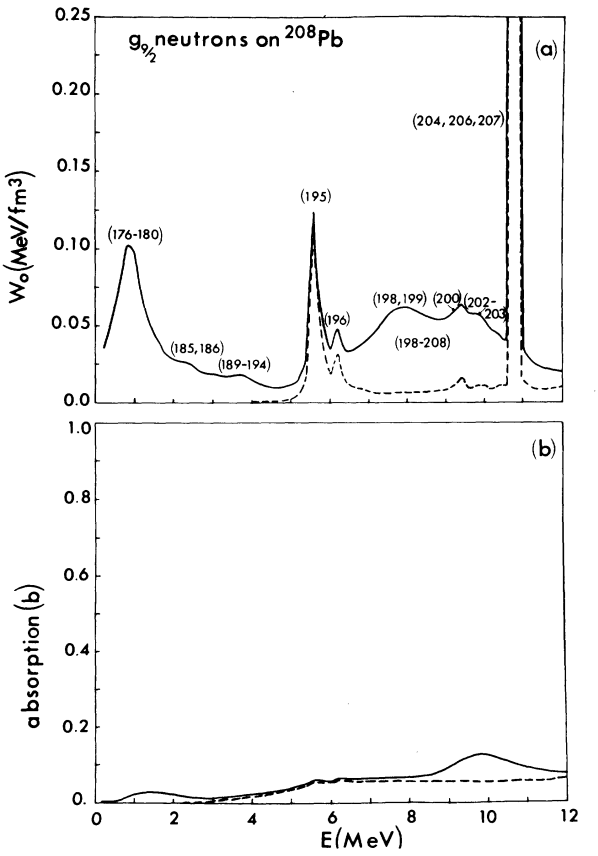

FIG. 9. Imaginary potential W_0 and absorption for $g_{9/2}$ neutrons. See Fig. 1 caption for details.

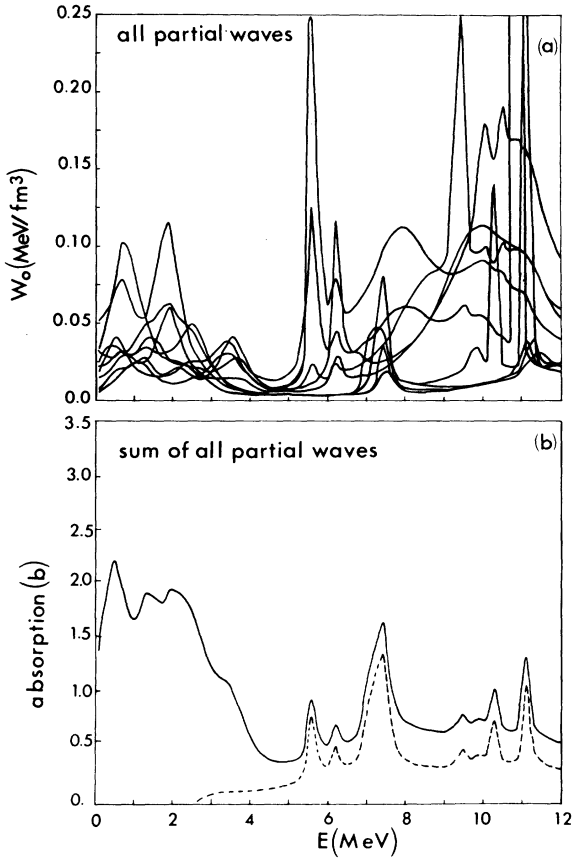

FIG. 10. Part (a) gives separately the imaginary potential peaks W_0 for $s_{1/2}$, $p_{1/2}$, $p_{3/2}$, $d_{3/2}$, $d_{5/2}$, $f_{5/2}$, $f_{7/2}$, $g_{7/2}$, and $g_{9/2}$ neutrons [cf. Figs. 1–9]. Part (b) gives the sum of the absorptions for these partial waves. The dashed line is the contribution of the inelastic excitations.

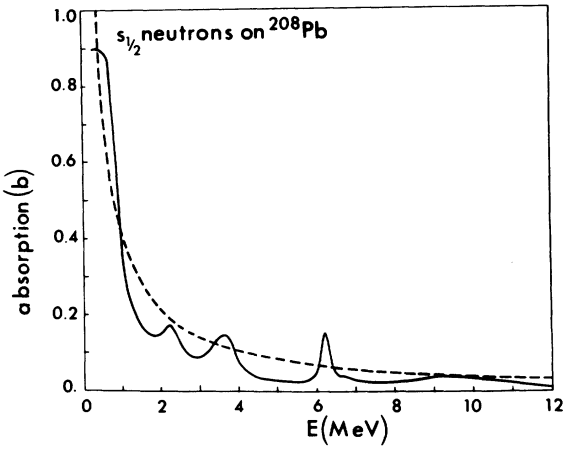

FIG. 11. Comparison for $s_{1/2}$ neutrons of the calculated absorption from the nonlocal energy-dependent potential with that obtained from a phenomenological local energy-independent potential, cf. Eq. (14). The strength of the local potential is 5 MeV. The solid line is the same as in part (b) of Figs. 1–9. The dashed curve represents the absorption due to the local potential.

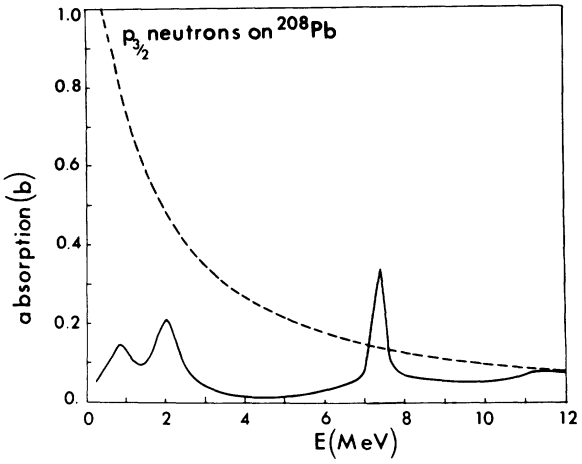

FIG. 13. Comparison for $p_{3/2}$ neutrons of the absorption calculated from our nonlocal potential and a phenomenological local potential. See Fig. 11 caption and text for details.

ever, because of the angular momentum barrier ($kR < l$) the g-wave functions are drastically reduced near the nuclear surface and consequently the cross section is expected to be quite small. In fact, for the energy range of interest one need not consider higher partial waves.

(6) Another way that the scattering wave functions can affect the absorption cross section is through the radial dependence of the wave functions. We have noted [Eq. (19)] that the imaginary optical potential has essentially the same radial dependence for all energies, i.e., surface peaked with a range β of about 1 fm. If the wavelength λ of the scattered wave functions is much bigger than β, then the cross section will vary only slightly with energy, and will be either large or small depending on the overlap of the scattering wave functions with the potential. If $\lambda \approx \beta$ then this overlap, and hence the cross section, could have a significant energy dependence. For $\lambda \ll \beta$ there are so many oscillations of the wave functions within the potential that the overlap is ex-

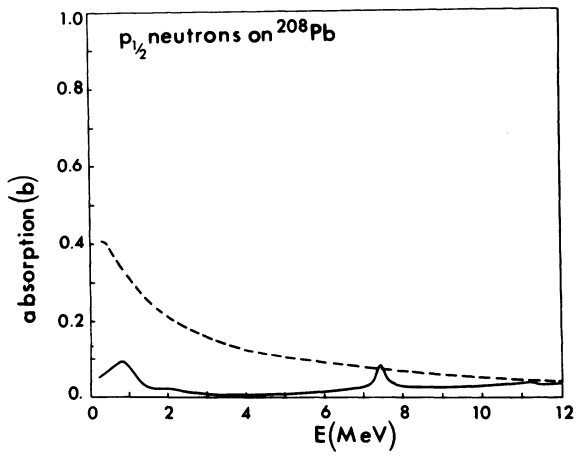

FIG. 12. Comparison for $p_{1/2}$ neutrons of the absorption calculated from our nonlocal potential and a phenomenological local potential. See Fig. 11 caption and text for details.

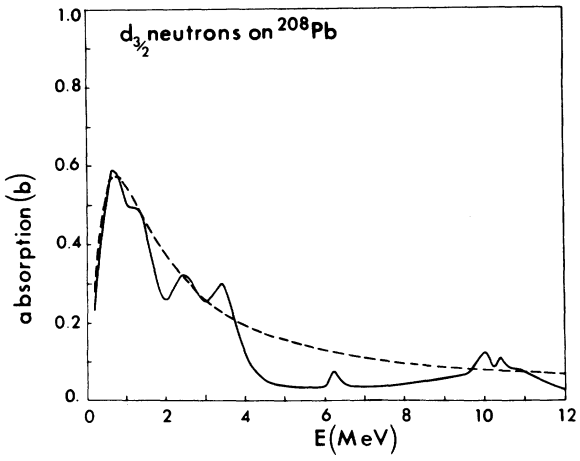

FIG. 14. Comparison for $d_{3/2}$ neutrons of the absorption calculated from our nonlocal potential and a phenomenological local potential. See Fig. 11 caption and text for details.

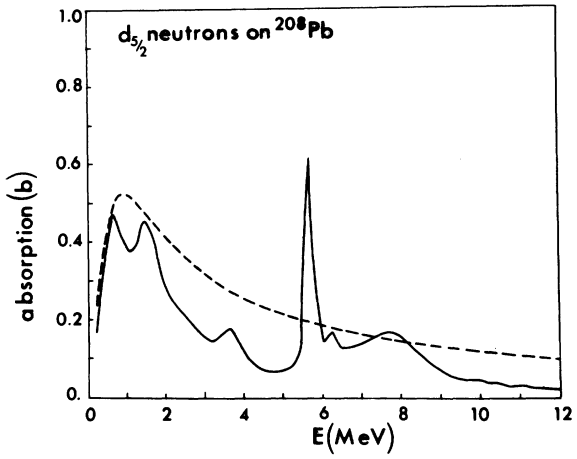

FIG. 15. Comparison for $d_{5/2}$ neutrons of the absorption calculated from our nonlocal potential and a phenomenological local potential. See Fig. 11 caption and text for details.

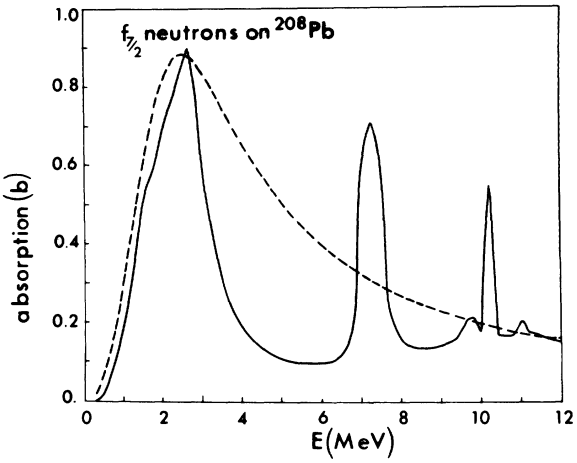

FIG. 17. Comparison for $f_{7/2}$ neutrons of the absorption calculated from our nonlocal potential and a phenomenological local potential. See Fig. 11 caption and text for details.

pected to be constant, and hence the cross section should have no significant energy dependence. The energy dependences described above are in addition to that referred to in item (5).

For the energy range 0–12 MeV the wavelength λ is greater than 8 fm and therefore $\lambda \gg \beta$ and the first-described situation prevails. Thus, while this situation could provide a slight energy dependence, it seems that the amplitude of the wave functions as discussed in item (5) is the more important effect.

(7) The general effect of the scattering wave function on the absorption cross section is easily seen from the dashed lines in Figs. 11–20. These lines give the cross section for an arbitrarily chosen phenomenological local energy-independent potential as described in Sec. III. Because of the properties of the wave function the cross section in most cases is not just a simple monotonically decreasing function of energy, but rather reflects the potential scattering resonance behavior of the wave function. This is in line with the general

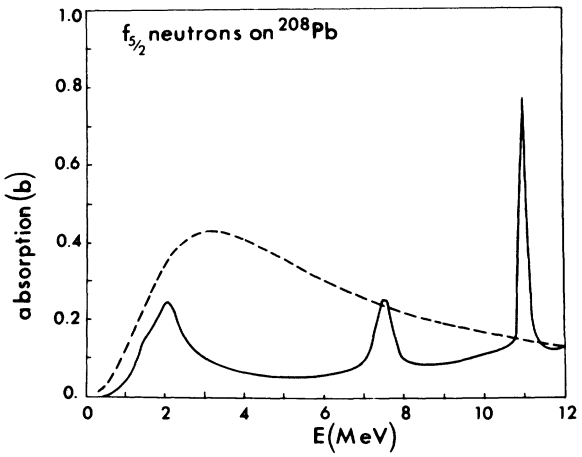

FIG. 16. Comparison for $f_{5/2}$ neutrons of the absorption calculated from our nonlocal potential and a phenomenological local potential. See Fig. 11 caption and text for details.

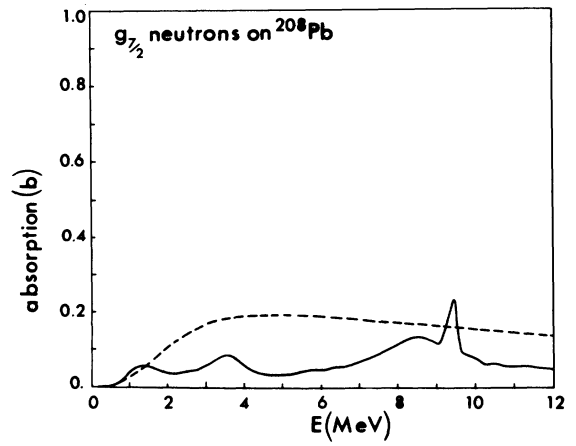

FIG. 18. Comparison for $g_{7/2}$ neutrons of the absorption calculated from our nonlocal potential and a phenomenological local potential. See Fig. 11 caption and text for details.

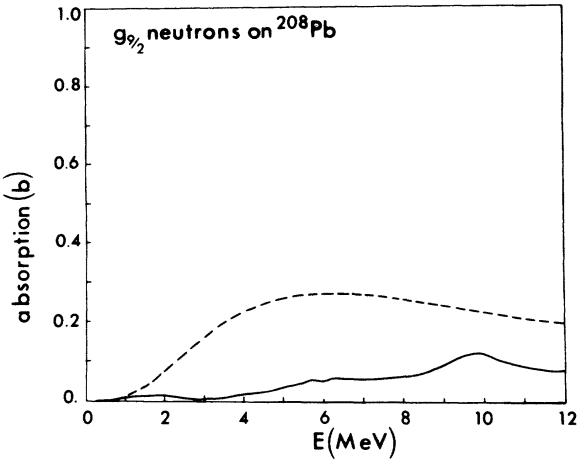

FIG. 19. Comparison for $g_{9/2}$ neutrons of the absorption calculated from our nonlocal potential and a phenomenological local potential. See Fig. 11 caption and text for details.

discussion in item (5). The actual positions of the resonances are sensitive to the depth of the real potential well used to generate the wave functions.

(8) While the phenomenological potential produces in some cases the general envelope of our calculated absorption, it cannot be expected to produce the detailed structure of the cross section. Such effects can only come from a more elaborate model, e.g., that of intermediate structure as employed in this paper.

(9) Figures 21–24 demonstrate that in general the calculated absorption cross sections agree very well with experiment. The comparison for s waves is quite good and has previously been reported by us.[15] In this case there are three doorways that contribute to the calculated cross section in Fig. 21(c), and the observed cross sections in Figs. 21(a) and 21(b) appear to have resonances corresponding to these doorways. The extra experimental resonance cannot be explained in our model.

For the higher partial waves in Figs. 22–24 it is the sum of the calculated cross sections, given in parts (c) and (d), that should be compared with experiment. However, for a given l value doorways of the same particle-vibration makeup and different j value are degenerate in our model. This degeneracy is expected to be removed by the residual interaction. Thus all the resonances appearing in parts (c) and (d) in each of Figs. 22–24 should be counted separately for comparison to experiment.

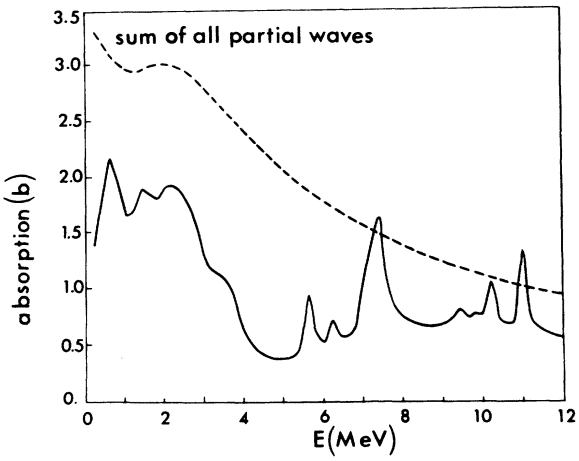

FIG. 20. Comparison of the total absorption calculated from our nonlocal potential (solid line) and a phenomenological local potential (dashed line). Partial waves $l=0$–4 are included. This is the sum of the cross sections of Figs. 11–19.

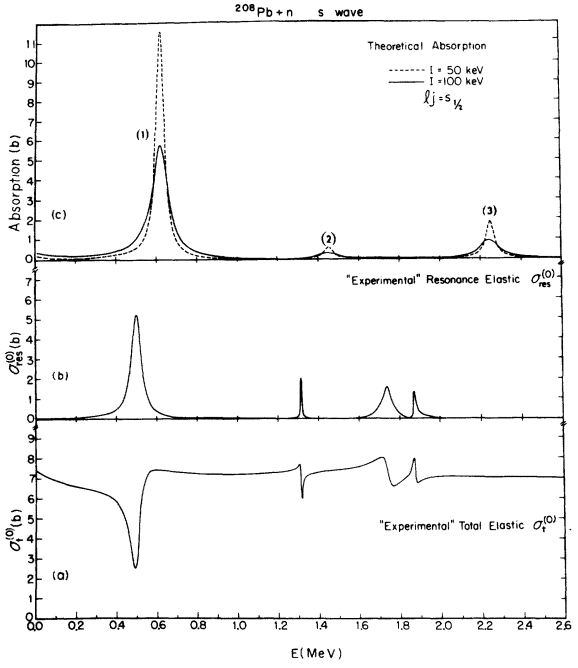

FIG. 21. Comparison of calculated and experimental cross sections for s waves. (a) Total s-wave experimental cross section (i.e., including both potential and resonance elastic scattering) as generated from an R-matrix code using parameters that fit the data of Farrell *et al.* (Ref. 25), Divadeenam *et al.* (Ref. 26), and Fowler (Ref. 27). The word experimental is in quotes to indicate that only the s-wave portion of the experimental cross section is shown. (b) R-matrix-generated resonance elastic cross section. The same parameters as in (a) are used. (c) Calculated absorption cross section.

In the case of p waves seven resonances are predicted in the absorption cross section, three for $p_{1/2}$ [Fig. 22(d)] and four for $p_{3/2}$ [Fig. 22(c)]. Experimentally, many more resonances are observed [Figs. 22(a) and 22(b)]. We found that the spreading of the doorways into more complicated states (e.g. 2 vibration-1 particle) cannot account for the extra levels seen in this energy range (0–2.2 MeV). However, the abundance of levels may be understood as follows. It is possible to construct many 2p-1h doorways of negative parity in the energy range of interest. This is because all of the low-lying available single-neutron states (except for $1j_{15/2}$) are of positive parity while all the neutron-hole states ($3p_{1/2}$, $2f_{5/2}$, $3p_{1/2}$ etc., except for $1i_{13/2}$) are of negative parity. Such noncollective doorways were not considered as part of our model; and thus we predict fewer levels than are observed experimentally for p waves. By contrast, it is very difficult to obtain a 2p-1h doorway of positive parity in this same energy range. The number of s-wave resonances in our model thus agrees well with experiment.

For d waves 11 resonances (of which 6 are quite strong) are predicted [Figs. 23(c) and 23(d)] while 7 resonances appear in the experimental absorption [Figs. 23(a) and 23(b)]. The resonances in the calculated cross section are clustered into two distinct energy groups, one group near about 0.6 MeV and one cluster near about 1.5 MeV. This clustering is in excellent agreement with experiment. The number of strong resonances in each cluster also agrees well with the observed number.

Finally, in the case of f waves there is also a good agreement with observation. In particular there are no experimental resonances up to about 1.4 MeV [Figs. 24(a) and 24(b)]. Up to this energy we predict [Figs. 24(c) and 24(d)] only two very weak degenerate resonances at 0.8 MeV. At about 1.4 MeV we predict three resonances, two of which are degenerate with the same particle-vibration constituents but different spin. These can be associated with the observed resonance at about 1.4 MeV. Above this energy theory predicts a distinct cluster of six levels (some of which are degenerate and four of which are strong) near about 2 MeV which can be associated with an ob-

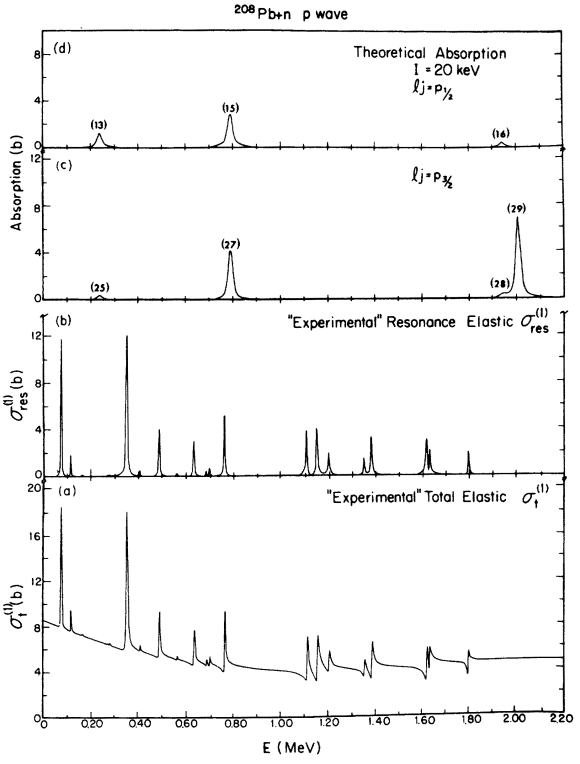

FIG. 22. Comparison of calculated and experimental cross sections for p waves. Parts (a) and (b) are as described in Fig. 21. Parts (c) and (d) give, respectively, the calculated $p_{3/2}$ and $p_{1/2}$ absorption cross sections.

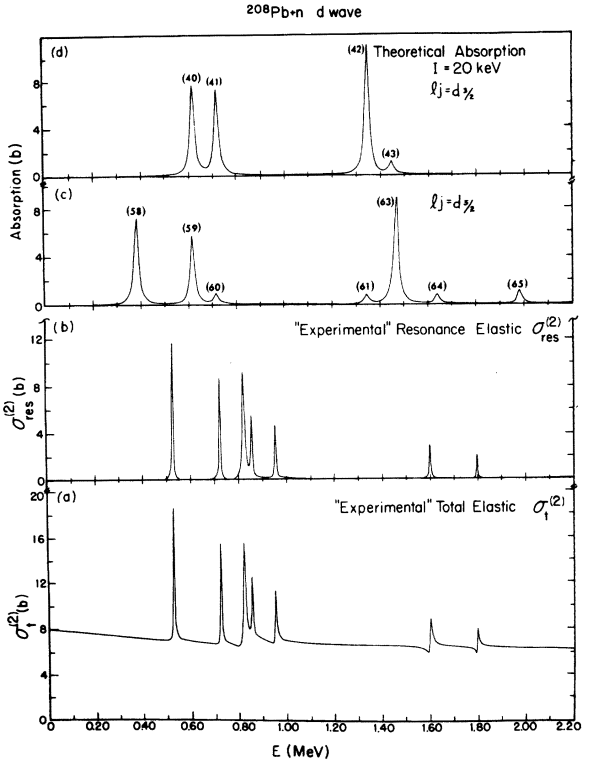

FIG. 23. Comparison of calculated and experimental cross sections for d waves. Parts (a) and (b) are as described in Fig. 21. Parts (c) and (d) give, respectively, the calculated $d_{5/2}$ and $d_{3/2}$ absorption cross sections.

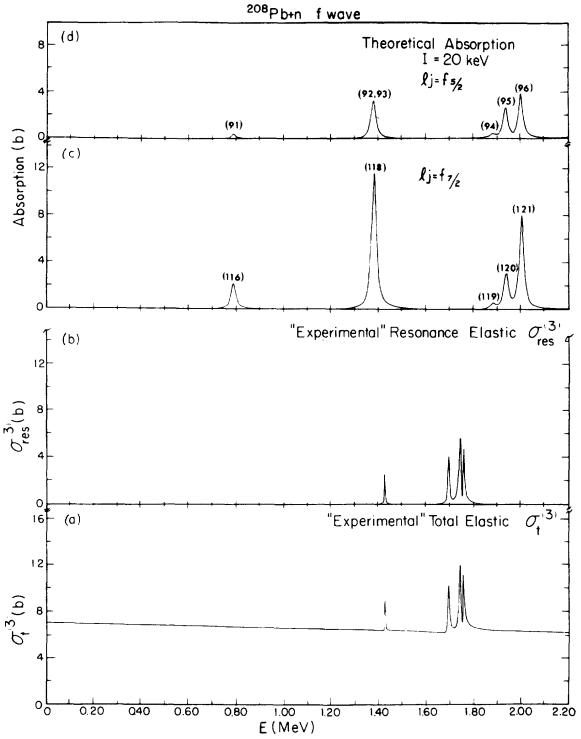

FIG. 24. Comparison of calculated and experimental cross sections for f waves. Parts (a) and (b) are as described in Fig. 21. Parts (c) and (d) give, respectively, the calculated $f_{7/2}$ and $f_{5/2}$ absorption cross sections.

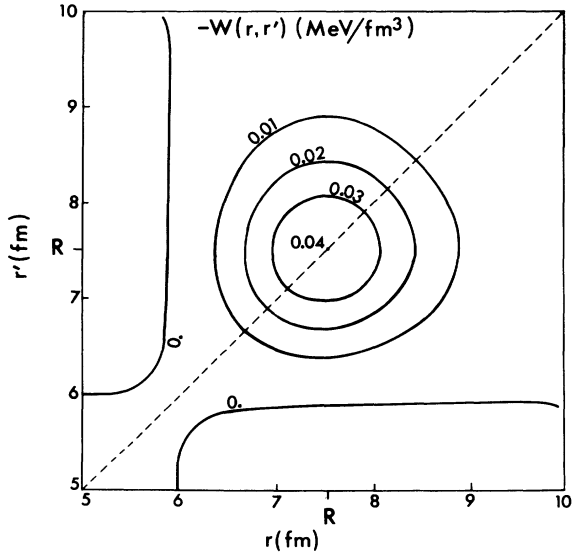

FIG. 25. Contour lines of $-W_{ljE}(r,r')$ [Eq. (13b)] for $lj = s_{1/2}$ and $E = 0.5$ MeV. The value of I is 0.75 MeV. The nuclear radius R is indicated. The dashed line is a symmetry axis. See text for details.

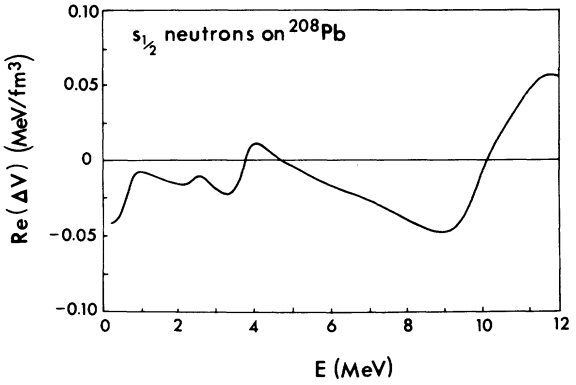

FIG. 26. Real part of the optical potential $\mathrm{Re}[\Delta V_{ljE}(R, R')]$ for $s_{1/2}$ neutrons. See text for details.

served group of three resonances near about 1.8 MeV.

One might expect as in the case of p waves that there would be many more observed f-wave resonances. However, because of the high angular momentum there is only a small overlap of the f-wave function with the nucleus at such low energies, and this diminishes the cross section. A similar argument was given in item (5) to explain the small g-wave absorption.

(10) Agreement with experiment would be improved by adjusting our single-particle energies and averaging width I. The single-particle energies control the position of the calculated resonances, while I is important for the detailed shape of the potential and the cross section. A smaller value of I leads to sharper and more easily resolved resonances.

(11) The calculated nonlocal contribution to the real potential for s waves (Fig. 26) has an alternating sign and, as expected, is relatively small. In fact, the calculated real potential is even smaller than the calculated imaginary potential (Fig. 1). The alternating sign implies that the contribution of our nonlocal real potential to the calculation of cross sections will be rather small.

(12) It is difficult to make a *direct* comparison between our calculated nonlocal imaginary potential and the usual phenomenological local potentials that appear in the literature. In order to make such a comparison our potential must be converted into an equivalent local potential. Such a procedure is presented in another publication.[28]

We thank Professor Carl Shakin for his interest in our work and for several helpful discussions and suggestions.

*Work supported by the U.S. Army Research Office, Durham, North Carolina.
†Work supported by the U. S. Atomic Energy Commission.

[1]F. Perey and B. Buck, Nucl. Phys. 32, 353 (1962).
[2]L. Rosen, J. G. Beery, and A. S. Goldhaber, Ann. Phys. (N. Y.) 34, 96 (1965).
[3]F. D. Becchetti, M.S. thesis, University of Minnesota, 1968 (unpublished).
[4]G. W. Greenlees, G. J. Pile, and Y. C. Tang, Phys. Lett. B26, 658 (1968); Phys. Rev. 171, 1115 (1968).
[5]F. D. Becchetti and G. W. Greenlees, Phys. Rev. 182, 1190 (1969).
[6]D. A. Slanina, Ph.D. thesis, Michigan State University, 1969 (unpublished).
[7]M. Bruneau and N. Vinh-Mau, in *Methods and Problems of Theoretical Physics* (North-Holland, Amsterdam, 1970).
[8]G. L. Payne, Phys. Rev. 174, 1227 (1968).
[9]J. Cugnon, Nucl. Phys. A208, 333 (1973).
[10]T. F. O'Dwyer, M. Kawai, and G. E. Brown, Phys. Lett. 41B, 259 (1972).
[11]C. L. Rao, M. Reeves, III, and G. R. Satchler, Nucl. Phys. A207, 182 (1973).
[12]G. R. Satchler, in Symposium on Correlations in Nuclei, Balatonfüred, Hungary, September 3–8, 1973 (unpublished).
[13]N. Azziz and R. Méndez-Plácido, Phys. Rev. C 8, 1849 (1973).
[14]C. Mahaux and H. A. Weidenmüller, *Shell Model Approach to Nuclear Reactions* (North-Holland, Amsterdam, 1969).
[15]A. Lev, W. P. Beres, and M. Divadeenam, Phys. Rev. Lett. 31, 555 (1973).
[16]H. Feshbach, A. K. Kerman, and R. H. Lemmer, Ann. Phys. (N. Y.) 41, 230 (1967).
[17]N. Auerbach, J. Hüfner, A. K. Kerman, and C. M. Shakin, Rev. Mod. Phys. 44, 48 (1972).
[18]B. R. Mottelson, J. Phys. Soc. Jap. Suppl. 24, 87 (1965).
[19]An alternative method to calculate the imaginary part of the integral for $E-E_\lambda > 0$ is to observe that in the limit $I \to 0$ the sum and integral in Eq. (8) are the spectral representation of the single particle Green's function $G_{l'j'}(E-E_\lambda; r, r')$. Only the integral contributes to the imaginary part, and this contribution can be evaluated by using the closed form of the Green's function.
[20]J. Blomqvist and S. Wahlborn, Ark. Fys. 16, 545 (1960).
[21]M. B. Lewis and F. E. Bertrand, Nucl. Phys. A196, 337 (1972).
[22]M. Divadeenam and W. P. Beres, Phys. Rev. C 8, 1123 (1973), and references therein.
[23]O. Nathan and S. G. Nilsson, in *Alpha-, Beta-, and Gamma-Ray Spectroscopy*, edited by K. Siegbahn (North-Holland, Amsterdam, 1965), Chap. X.
[24]G. R. Satchler, Nucl. Phys. A195, 1 (1972).
[25]J. A. Farrell, G. C. Kyker, E. G. Bilpuch, and H. W. Newson, Phys. Lett. 17, 286 (1965).
[26]M. Divadeenam, W. P. Beres, J. A. Farrell, G. C. Kyker, E. G. Bilpuch, and H. W. Newson, to be published.
[27]J. L. Fowler, Phys. Rev. 147, 870 (1966).
[28]A. D. Mackellar, R. E. Schenter, H. M. Schadel, W. P. Beres, and A. Lev, Complex Local Equivalents to Imaginary Nonlocal Optical Potentials: Neutron Scattering from ^{208}Pb (to be published).